Science of Sintering, **50** (2018) 39-50

doi: https://doi.org/10.2298/SOS1801039V

UDK 546.824; 622.785

Structure and photocatalytic properties of sintered TiO_2 nanotube arrays

Jelena Vujančević[1*)], Anđelika Bjelajac[2], Jovana Ćirković[3], Vera Pavlović[4], Endre Horvath[5], László Forró[5], Branislav Vlahović[6,7], Miodrag Mitrić[8], Đorđe Janaćković[9], Vladimir Pavlović[1]

[1]Institute of Technical Science of SASA, Knez Mihailova 35/IV, 11000 Belgrade, Serbia

[2]University of Belgrade, Innovation Center of the Faculty of Technology and Metallurgy, Karnegijeva 4, 11120 Belgrade, Serbia

[3]University of Belgrade, Institute for Multidisciplinary Research, Kneza Višeslava 1, 11030 Belgrade, Serbia

[4]University of Belgrade, Faculty of Mechanical Engineering, Kraljice Marije 16, 11120 Belgrade 35, Serbia

[5]École Polytechnique Fédérale de Lausanne, Laboratory of Physics of Complex Matter (LPMC), 1015 Lausanne, Switzerland

[6]North Carolina Central University, Department of Physics, 1801 Fayetteville St Durham, North Carolina 27707, USA

[7]NASA University Research Center for Aerospace Device Research and Education and NSF Centre of Research Excellence in Science and Technology Computational Center for Fundamental and Applied Science and Education, North Carolina, USA

[8]University of Belgrade, Vinča Institute of Nuclear Sciences, P.O.Box 522, 1101 Belgrade, Serbia

[9]University of Belgrade, Faculty of Technology and Metallurgy, Karnegijeva 4, 11000 Belgrade, Serbia

Abstract:

One-dimensional (1D) TiO_2 nanotubes perpendicular to the substrate were obtained by electrochemical oxidation of titanium foil in an acid electrolyte. In order to alter the crystallinity and the morphology of films the as-anodized amorphous TiO_2 nanotube films were sintered at elevated temperatures. The evolution of the morphology was visualized via scanning electron microscopy (SEM), while the crystalline structure was investigated by X-ray diffraction (XRD) and Raman spectroscopy. The chemical composition was studied by X-ray photoelectron spectroscopy (XPS). The effects of crystallinity and morphology of TiO_2 nanotube (NTs) films on photocatalytic degradation of methyl orange (MO) in an aqueous solution under UV light irradiation were also investigated. The TiO_2 nanotubes sintered at 650 °C for 30 min had the highest degree of crystallinity and exhibited the best photocatalytic activity among the studied TiO_2 nanotube films.

Keywords: *Titanium dioxide; Anodization; Sintering; Crystal phase; Photocatalysis.*

*) **Corresponding author:** jelena.vujancevic@itn.sanu.ac.rs

1. Introduction

Processes for sustainable environmental protection, such as wastewater treatment, air purification and decomposition of undesirable compounds have become a great demand in modern society. Photocatalyst has been introduced with the aim of developing clean chemical processes and environmentally friendly materials that will degrade harmful pollutants into non-toxic substances.

Photocatalysts are semiconductors that use the energy of light to facilitate the decay of organic and inorganic pollutants. Among the variety of semiconductors, such as TiO_2, ZnO [1], ZrO [2], ZnS [3], MoS_2 [4], titanium dioxide has become the most commonly used photo-induced catalyst due to its strong oxidizing capacity [5], chemical stability, nontoxicity and photocorrosion resistance.

Many factors influence the photocatalytic performance of TiO_2, e.g. structural dimensionality, size, specific surface area, pore structure and crystalline phase [6]. A high specific surface area and a unidirectional channel for charge carrier transport can be achieved by synthesizing one-dimensional nanoarrays. This provides a faster electron transport, reducing carrier recombination and improving photocatalytic activity [6].

Along with dimensionality, crystal structure plays an important role in the photocatalytic performance. TiO_2 has three main crystalline structures: anatase, rutile and brookite. Anatase and rutile are more efficient in photocatalysis. Rutile has a lower band gap (3.0 eV) than anatase (3.2 eV), and it is expected to show better photocatalytic activity. According to previous studies [7-9], rutile turned out to be less efficient than anatase in the degradation of a large number of organic molecules. Sun et al. [10] showed that pure anatase TiO_2 nanotubes annealed at 450 °C exhibited the highest photoconversion efficiency of 4.49 % and the maximum hydrogen production rate of 122 μmol/(hcm^2). Oh et al. [11] demonstrated that the anatase type TiO_2 nanotubular film annealed at 550 °C had the best photocatalytic performance in the photodegradation of aniline blue. On the other hand, there are publications showing that rutile exhibits a higher photocatalytic activity than anatase in the decomposition of methylene blue, due to its higher crystallinity [12]. Furthermore, it seems that, compared to pure anatase or rutile, mixed-phase TiO_2 shows a higher photocatalytic activity, which is directly related to the surface-phase structure and the phase junction formed between anatase and rutile [13]. Yu et al. [14] observed the highest photocatalytic activity and the highest formation rate of hydroxyl radicals and photocurrent in the nanotubular TiO_2 annealed at 600 °C, due to its biphasic structure and good crystallization. Therefore, there is a need for a more detailed insight into the temperature transition of TiO_2 polymorphs and their influence onto the photocatalytic performance.

It has been established that the temperature of the transition from metastable anatase to stable rutile depends on many factors, such as particle size, lattice strain, morphology, impurities in the lattice [15]. In this article, the stability of the structure, tube geometries and the crystal phase transformations upon sintering were investigated. The effect of these parameters on the photocatalytic activity of TiO_2 nanotube films was also determined.

2. Experimental procedure

Commercial titanium foils (1 × 2.5 cm^2, 0.25 mm thick, 99.7 %, Aldrich) were cleaned in an ultrasonic bath with acetone, ethanol and deionized water, successively. After drying, the foils were immersed in 1.27 wt.% HF and 0.53 wt.% CH_3COOH containing electrolyte along with platinum foil that served as a cathode. The distance between the electrodes was 1 cm. Anodization was performed at a potential of 15 V for 30 minutes, with continuous stirring of the electrolyte. The samples were dried in air and then annealed at 450, 600, 650 and 700 °C, in the air for 30 minutes, with a heating rate of 5 °Cmin^{-1}.

The morphology evolution was studied using scanning electron microscopy (FEI NanoSEM 630, 15keV).

Raman spectra were obtained in the range from 100 to 1100 cm^{-1}, with a Horiba Jobin Yvon Aramis Raman/PL System, using a He-Ne laser operating at 632.8 nm with the power of 1 mW on the sample surface. All measurements were performed using a grating with 1800 lines/mm, a 100× microscope objective and the acquisition of 10s/5 cycles.

The X-ray Diffraction (XRD) patterns were obtained on a Philips PW-1050 diffractometer, operated at 40 kV and 30 mA, using Ni-filtered Cu K_α radiation (1.5419 Å). Bragg–Brentano focusing geometry was used with a fixed 1° divergence and 0.1° receiving slits. The patterns were taken in the 20–80° 2θ range with the step of 0.05° and collection time of 1 s per step. The crystalline sizes were estimated using Scherrer's equation [16] $D = k/(\beta\cos\theta)$, where D was crystalline size, k the Sherrer's constant, λ the wavelength of X-ray radiation, β the full-width at half-maximum (FWHM) and θ was the diffraction angle.

The XPS measurements were conducted on a Kratos Axis Ultra XPS system with Monochromated Aluminum K-Alpha X-Rays ($h\nu$ = 1486,6 eV). During the measurement, chamber vacuum was at 2.5×10^{-8} torrs. The X-Ray gun was operated at 15 kW and 10 mA. A charge neutralizer was used to reduce the charging effects from non-conducting surfaces. All survey scans were collected with a Pass Energy of 160 eV and one sweep (or averaging). All Region scans were made with a Pass Energy of 20 eV, and the number of sweeps (averages) performed was dependent on the measured region. All data was calibrated to the C-C portion of the C1s peak at 284.5 eV.

The photocatalytic activity of TiO_2 nanotube films on titanium foil was investigated by immersing the samples into 3 ml of aqueous MO solution (concentration of 5 mg/L). In order to the achieve adsorption/desorption equilibrium, the samples were left in solution for 1 h in the dark prior to the photocatalytic test reaction. The sample was illuminated by a spot light source (Hamamatsu LC5) from a distance of 1 cm (light intensity 5.2 mW/cm^2). The decomposition rate of MO as a function of irradiation time was measured by a Varian Cary 50 Scan UV-Vis spectrophotometer. In order to determine the intrinsic photolysis of MO (i.e. the UV light-induced self-decomposition), the aqueous solution of MO without photocatalysts was irradiated.

3. Results and Discussion

The anodization of Ti foil is a promising approach to fabricating vertically oriented TiO_2 nanotube arrays directly grown on the Ti substrate, without a template. The sintering temperature is an important parameter that affects the morphology and crystallinity of nanotubes. Fig. 1 (a-j) shows the evolution of the nanotube morphology as a consequence of sintering temperature change. Tab. I shows the influence of the annealing temperature on the average inner diameter (*Di*), the wall thickness (*W*) and the tube length (*L*) obtained using the image analysis software. The porosity was calculated according to the equation [17]:

$$P = 1 - \frac{2\pi W(Di + W)}{\sqrt{3}(Di + 2W)^2}$$

Fig. 1a and b show well-defined TiO_2 nanotubes formed in an aqueous solution of HF at a potential of 15 V. It is evident that the highly ordered nanotube array consists of very regular tubes with an average inner diameter of 90 nm and a wall thickness of 10 nm. The length of the tubes is 315 nm, with rough walls typical of nanotubes grown in an electrolyte with water [18]. After annealing at 450 °C, nanotubular arrays retained their structural integrity, with a slight change in the diameters, wall thickness and length, as it is shown in Tab. I. At 600 °C, a compact layer appeared at the interface between the TiO_2 nanotubes and

the titanium foil and due to that the length of nanotubes decrease on L = 220 nm. With further increase in temperature, the diameters slightly decreased, while the length shortened drastically. This can be presumably ascribed to the sintering process that occurs during crystallization. At 700°C, nanotubes no longer had a regular shape, with recognizable particles grown from the nanotubes. With sintering, the porosity lowered (Tab. I) due to the shrinking of the tubes, which merged together, reducing the spacing between the walls.

Tab. I Average morphological parameters for as-anodized and sintered TiO_2 nanotubes.

Samples	***D_i (nm)***	***W (nm)***	***L (nm)***	***P***
As-anodized	90	10	314	0.70
450 °C	75	13	315	0.60
600 °C	84	13	222	0.62
650 °C	72	16	152	0.53
700 °C	/	/	105	/

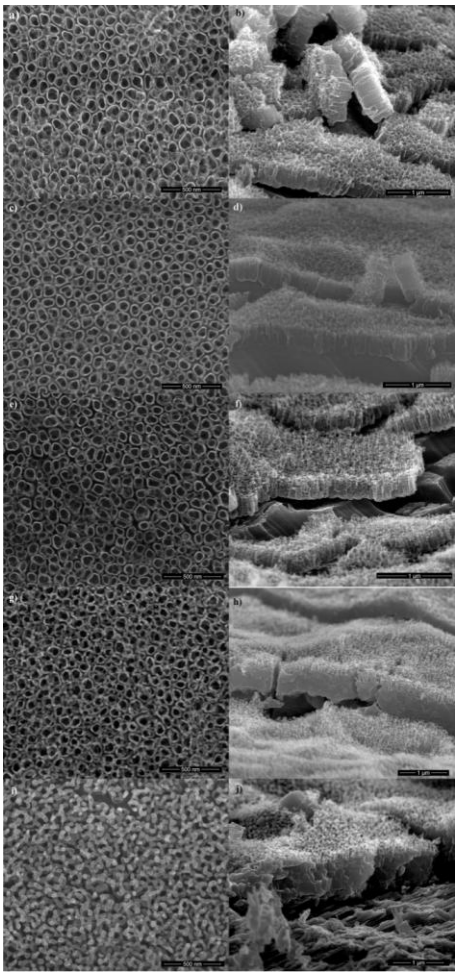

Fig. 1. SEM micrographs of the top and side views of TiO_2 nanotubes sintered at different temperatures: (a and b) as-anodized, (c and d) 450 °C, (e and f) 600 °C, (g and h) 650 °C, (i and j) 700 °C.

In order to determine the phase composition and crystallinity of TiO_2 nanotube arrays at different sintering temperatures, the XRD diffractograms and Raman spectra were studied. Fig. 2 shows the diffractograms of TiO_2 nanotube arrays annealed at a different temperature. The as-anodized TiO_2 nanotubes are amorphous, due to which only the peaks of the titanium substrate are present in the diffractogram. With annealing, TiO_2 nanotubes crystallized in two polymorphous forms: anatase and rutile. At 450 °C, anatase was observed as the main crystal phase due to the presence of two main anatase peaks at 25.3° and 48°, corresponding to the (101) and (200) planes, respectively. Also, a small amount of the rutile phase appeared at 27.3° (110). All other peaks came from the substrate, which dominated due to the low thickness of the film. Mor at al. [19] reported that in nanotubes on a titanium substrate, rutile appeared at 430 °C, while in nanotubes on conductive glass annealed at 500 °C rutile did not appear. This happened due to the growth of rutile crystallites at the interface between the nanotube bottom and the thermally oxidized Ti substrate [7]. With temperature rise to 600 °C, new peaks appeared at 36.1° (101), 41.4° (111), 44° (210), 54.3° (211), 56.7° (220) and 68.9° (301), which corresponded to the rutile phase. With further temperature increase up to 650 and 700 °C the intensity of the rutile peaks gradually strengthened, while the intensity of peaks from anatase decreased, proving that almost all anatase transformed into rutile. A decrease of the diffraction intensity of the titanium foil was also observed, revealing the crystallization of the support [20]. The phase composition and the crystallite size estimated using Scherrer's formula are shown in Tab. II. The crystal size of anatase and rutile was growing until the temperature reached 650 °C, when it started to drop, probably due to the collapse of the nanotube structure.

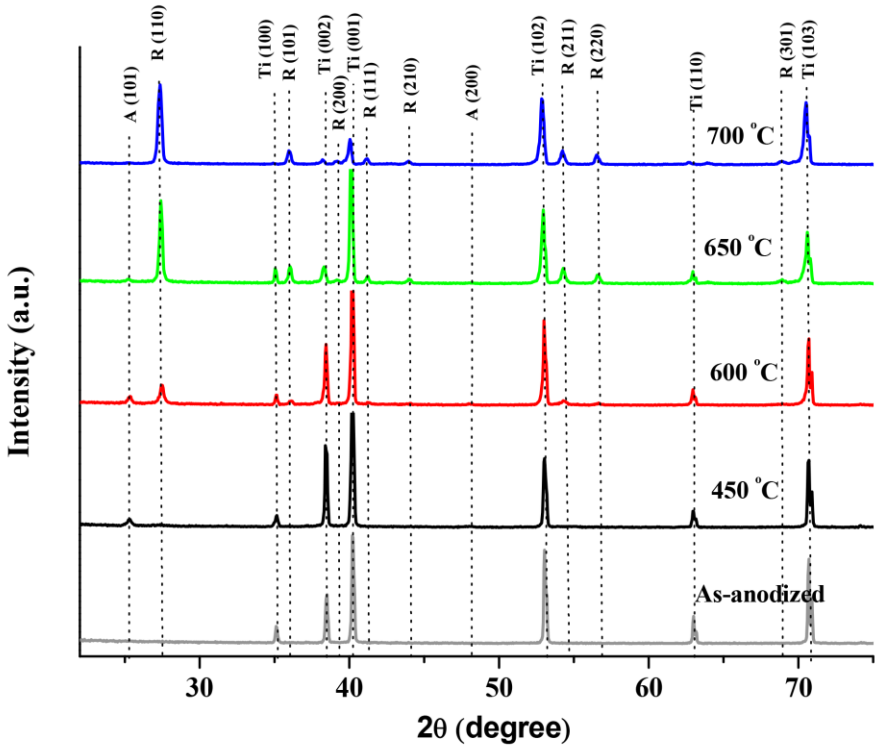

Fig. 2. XRD patterns of the as-anodized and sintered TiO_2 nanotubes (A-anatase, R-rutile, Ti-titanium).

Tab. II Phase composition and average crystallite size of annealed TiO_2 nanotubes.

Temperature of annealing, °C	Amount of anatase phase, %	Amount of rutile phase, %	Crystallite size for anatase (101)	Crystallite size for rutile (110)
450	99.7	0.3	23.1	5.4
600	20.3	79.7	28.9	25.7
650	2.5	97.5	26.2	34.6
700	0.6	99.4	24.2	27.3

The temperature-induced anatase and rutile crystal modifications of TiO_2 were tracked using spectroscopy methods. The Raman spectrum of the sample annealed at 450 °C (Fig. 3) showed only the Raman peaks characteristic for the crystal modification of anatase: at ~145 cm^{-1} ($E_{g(1)}$ mode), ~198 cm^{-1} ($E_{g(2)}$ mode) and ~395 cm^{-1} ($B_{1g(1)}$ mode), as well as the peak at ~515 cm^{-1} that corresponds to the superposition of the A_{1g} and $B_{1g(2)}$ modes and the peak at ~635 cm^{-1}, which comes from the $E_{g(3)}$ mode [21-23]. With an increase in temperature, new peaks started to appear in the Raman spectra, along with anatase peaks. At 600 °C, the rutile E_g mode at 425 cm^{-1} occurred, besides the anatase modes. Further temperature increase, up to 650 °C, resulted in more intensive rutile peaks, while the intensity of all the major anatase modes decreased and only the main anatase mode at ~145 cm^{-1} remained clearly visible.

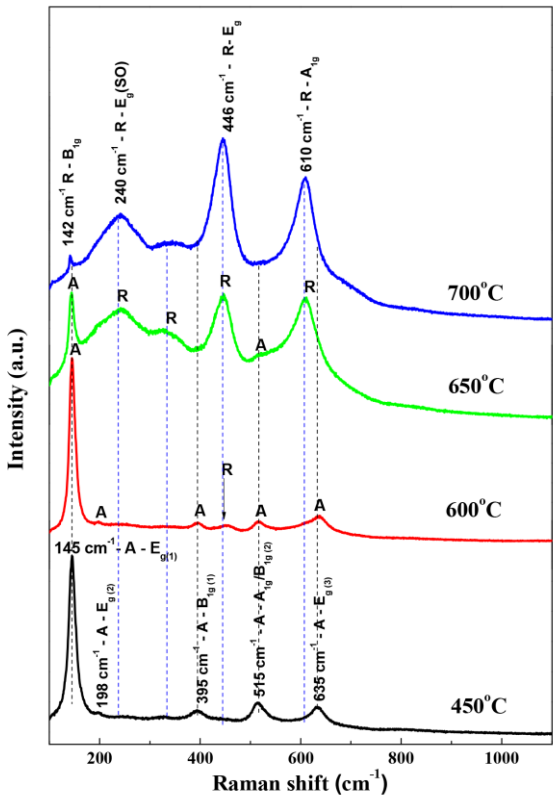

Fig. 3. Raman spectra of annealed TiO_2 nanotubes (A-anatase, R-rutile).

The rutile phase was observed as the dominant one, identified by the E_g mode at ~446 cm^{-1} and A_{1g} mode at 609 cm^{-1}, as well as by the broad peak at 242 cm^{-1}, which originated from

the second-order vibrational mode E_g (SO) and disorder effects [24, 25]. At 700 °C, the main anatase mode was replaced with the rutile B_{1g} mode at ~142 cm^{-1}, indicating that anatase phase completely disappeared. The whole spectrum at this temperature was assigned to the rutile phase, where the four Raman modes were prominent enough (B_{1g}, E_g, A_{1g} and E_g (SO)), while the mode expected at 826-827 cm^{-1} was too weak to be observed.

An XPS study was further employed in order to investigate how different annealing temperatures influenced the chemical composition of anodized titanium foil. The results are presented in Fig. 4. In pristine TiO_2, titanium (Ti 2p), oxygen (O1s), carbon (C1s), nitrogen (N1s), fluoride (F1s) and lead (4f) XPS peaks were noticed. After a heat treatment, peaks of lead, fluoride and nitrogen disappeared, proving that they were caused by surface contamination. No significant changes were noticed for the samples annealed at 450 and 600 °C, relative to pristine samples. Since the positions of Ti $2p_{3/2}$ and Ti $2p_{1/2}$ peaks (Fig. 5) in these samples ranged from 458.16 to 458.37 eV, and from 463.85 to 464.10 eV, respectively, it clearly indicated the existence of a Ti^{4+} state [26, 27]. Moreover, the difference in the binding energy of Ti $2p_{3/2}$ and Ti $2p_{1/2}$ peaks in all of the annealed samples was in accordance with the literature data for the mentioned state of titanium. Although at higher annealing temperatures both peaks shifted slightly towards lower binding energies, their positions still remained well above the binding energy of the Ti^{3+} state [27, 28]. In the O1s regions of binding energy, the peak at 529.6-529.7 eV proved O-Ti^{4+} bonding (Fig. 6) [29]. It was possible to assign it to the lattice oxygen in TiO_2. On the other hand, the shoulder effect that could be fitted with the peak at 531.0 ± 0.2 eV probably originated from surface-adsorbed oxygen (within the hydroxyl groups at the outermost surface, as well as within the adsorbed water resulting from moisture adsorption in air) [29]. The increase in annealing temperature up to 650 °C caused the reduction of the surface-adsorbed oxygen content. The atomic ratio O_{latt}/Ti2p provides an insight into the stoichiometry of the structure.

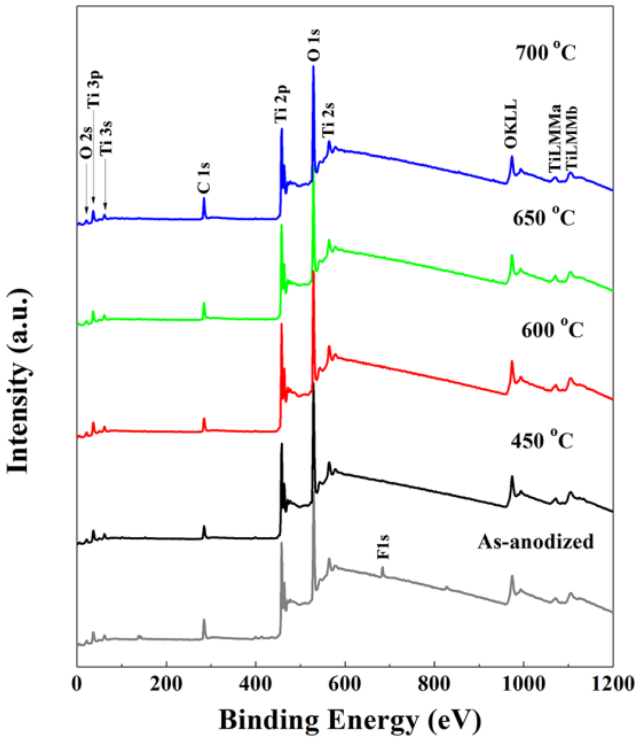

Fig. 4. XPS survey spectrum for as-anodized TiO_2 and sintered TiO_2.

The results show the substoichiometric structure for the amorphous (as-anodized) sample (Tab. III), which probably indicates the presence of oxygen vacancies in it. It can be assumed

that after annealing, the filling of oxygen defects proceeded, which was assisted by the crystallization process, since annealing was taking place in air.

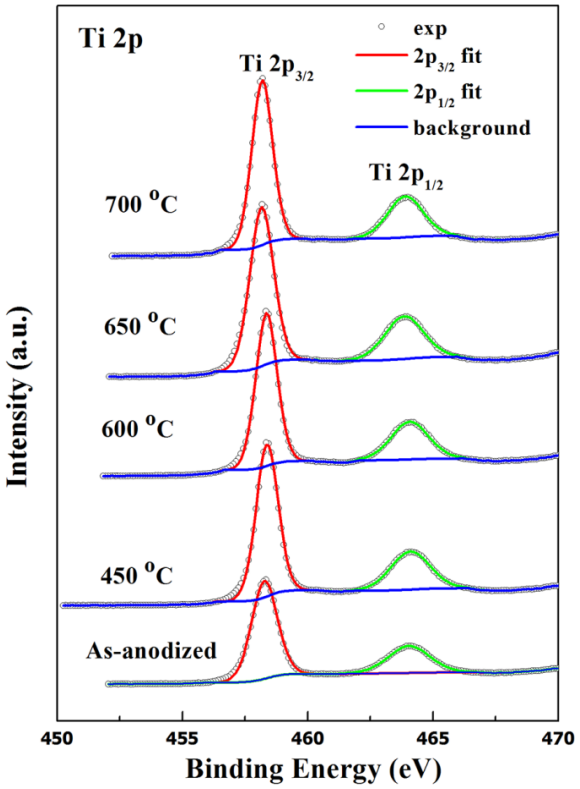

Fig. 5. XPS spectrum for Ti 2p peak for as-anodized and sintered TiO_2.

Tab. III XPS results of as-anodized and sintered TiO_2.

Samples	**O_{latt}/O_{tot} (area %)**	**O_{ads}/O_{tot} (area %)**	**O_{latt}/Ti2p (atomic ratio)**	**BE(Ti2p$_{1/2}$)-BE(Ti2p$_{3/2}$) (eV)**
As-anodized	58.7	41.3	1.6	5.77
450 °C	79.9	20.1	2.1	5.73
600 °C	82.0	18.0	2.1	5.72
650 °C	84.3	15.7	2.1	5.69
700 °C	81.5	18.5	2.1	5.72

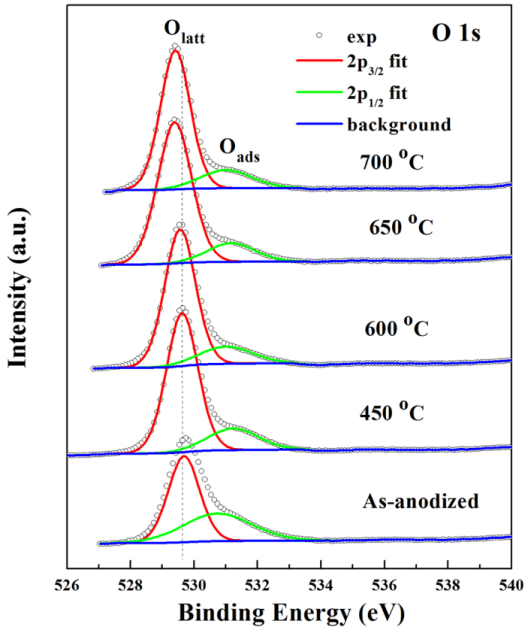

Fig. 6. XPS spectrum for O 1s peak for as-anodized and sintered TiO_2.

Tab. IV Influence of sintering temperature on photocatalytic degradation – first-order rate constant and correlation coefficient.

Temperature of annealing, °C	**$\|k\|$ x 10^{-2}, min^{-1}**	**R^2**
450	1.09	0.96
600	1.11	0.98
650	1.24	0.94
700	0.62	0.90

The influence of the sintering temperature of TiO_2 nanotubes on the degradation of the MO textile dye is shown on Fig. 7a. A further analysis indicated that the reaction could be presented as $\ln(C/C_o) = \ln(A/A_o) = kt$, where C_o was the initial dye concentration, C was the concentration after irradiation for time t. A_o and A were the corresponding absorbance, while k was a rate constant. Fig. 7b shows the linear curves proving that the degradation of MB by sintered TiO_2 nanotubes follows the pseudo-first order kinetic. The first-order constant k and the correlation coefficient R^2 are shown in Tab. IV. It is evident that an increased annealing temperature was accompanied by the increase of k, up to 700 °C, when it began to decrease gradually. The samples sintered at 450 °C and 600 °C had similar morphology parameters but there was a difference in the crystal structure. The reason for a higher kinetic constant for the sample annealed at 600 °C was probably the presence of the rutile phase. The best photocatalytic activity shows sample annealed at 650 °C due to the optimum ratio of anatase/rutile phase. The worst photocatalytic performance was exhibited by the sample annealed at 700 °C and this can be explained by the collapse of the nanotubular morphology and porosity loss, combined with the disappearance of the anatase phase (Fig. 2). The advantages of the mixed anatase-rutile phase could be due to the efficient trapping and

separation of photogenerated charges at the phase junction or the separation of the charges across different crystallite phases [30].

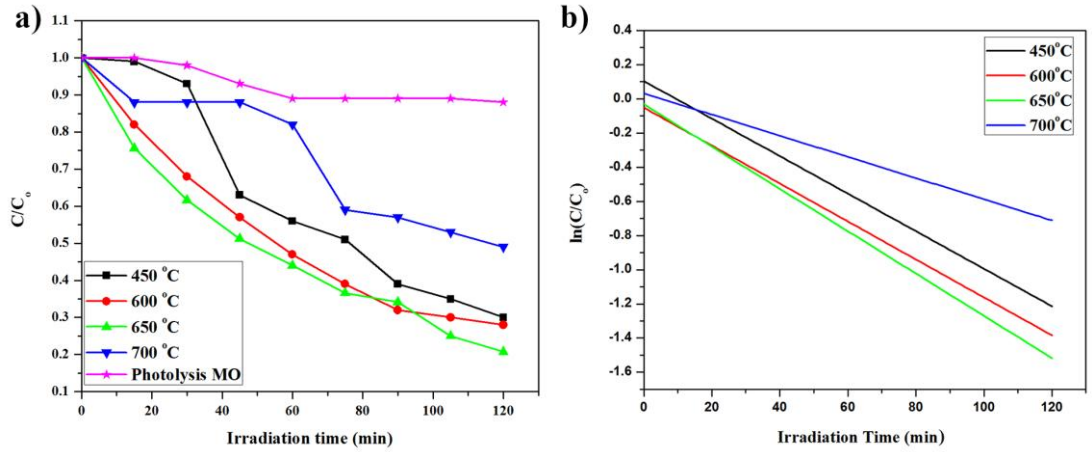

Fig. 7. Effect of sintered TiO_2 nanotubes on the photocatalytic MO degradation (a) and photocatalytic kinetic behavior of the degradation of MO by sintered TiO_2 nanotubes (b).

4. Conclusions

In this study, a highly ordered TiO_2 nanotube array on a Ti substrate was successfully fabricated using electrochemical anodization. It was observed that the morphologies and crystallinity of the TiO_2 nanotube array were greatly influenced by the sintering temperature. It was shown the sample annealed at 450 °C consisted mostly of the anatase phase, while 99.4 % of rutile was formed at 700 °C. At the temperatures of 600 °C and 650 °C, a mixture of anatase and rutile was observed. Different amounts of the polymorph phase strongly influenced the photodegradation of the MO dye. It was established that the TiO_2 nanotube array sintered at 650 °C showed the best photocatalytic activity, due to the optimal anatase-to-rutile ratio. With a further increase in temperature, up to 700 °C, the photocatalytic activity drastically decreased due to the collapse of the nanotubular structure and the excessive rutile content. As a result of the presented investigation, an appropriate tailoring of the ratio of polymorph phases in TiO_2 nanotubes could lead to a more suitable photocatalyst.

Acknowledgements

This research was supported by the project OI 172057 and project III 45019 of the Ministry of Education, Science and Technological Development of the Republic of Serbia, and by: NSF CREST (HRD-0833184), NASA (NNX09AV07A) and NSF-PREM1523617 awards. The work in Lausanne was supported by grants from Switzerland through the Swiss Contribution (SH/7/2/20). E. H. wants to thank the AIT grant, the Zeno-Karl Schindler foundation and MBR Global Water Initiatives for their support.

5. References

1. X. Chen, Z. Wu, D. Liu, and Z. Gao, Nanoscale Res. Lett., 12, 1 (2017) 143.
2. E. Bailón-García, A. Elmouwahidi, F. Carrasco-Marín, A. F. Pérez-Cadenas, and F. J.

Maldonado-Hódar, Appl. Catal. B Environ., 217 (2017) 540-550.
3. H. Zhang, X. Chen, Z. Li, J. Kou, T. Yu, and Z. Zou, J. Phys. D. Appl. Phys., 40, 21 (2007) 6846-6849.
4. M. Sabarinathan, S. Harish, J. Archana, M. Navaneethan, H. Ikeda, and Y. Hayakawa, RSC Adv., 7, 40 (2017) 24754-24763.
5. M. R. Hoffmann, S. T. Martin, W. Choi, and D. W. Bahnemann, Chem. Rev., 95, 1 (1995) 69-96.
6. K. Nakata and A. Fujishima, J. Photochem. Photobiol. C Photochem. Rev., 13, 3 (2012) 169-189.
7. D. Fang, Z. Luo, K. Huang, and D. C. Lagoudas, Appl. Surf. Sci., 257, 15 (2011) 6451-6461.
8. J. M. Macak, M. Zlamal, J. Krysa, and P. Schmuki, Small, 3, 2 (2007) 300-304.
9. Y. Lai, L. Sun, Y. Chen, H. Zhuang, C. Lin, and J. W. Chin, J. Electrochem. Soc., 153, 7 (2006) D123.
10. Y. Sun, K. Yan, G. Wang, W. Guo, and T. Ma, J. Phys. Chem. C, 115, 26 (2011) 12844-12849.
11. H. J. Oh, J. H. Lee, Y. J. Kim, S. J. Suh, J. H. Lee, and C. S. Chi, Appl. Catal. B Environ., 84, 1–2 (2008) 142-147.
12. N. Masahashi, Y. Mizukoshi, S. Semboshi, and N. Ohtsu, Appl. Catal. B Environ., 90,1–2 (2009) 255-261.
13. J. Zhang, Q. Xu, Z. Feng, M. Li, and C. Li, Angew. Chemie Int. Ed., 47, 9 (2008) 1766-1769.
14. J. Yu and B. Wang, Appl. Catal. B Environ., 94, 3–4 (2010) 295-302.
15. O. Carp, C. L. Huisman, and A. Reller, Prog. Solid State Chem., 32, 1–2 (2004) 33-177.
16. B. D. Cullity, Elements of x-ray diffraction. Reading, MA: Addison-Wesley Publishing Company, Inc., 1978.
17. A. G. Kontos et al., Chem. Phys. Lett., 490, 1–3 (2010) 58-62.
18. Z. Su and W. Zhou , J. Mater. Chem., 21, 25, (2011) 8955.
19. G. K. Mor, O. K. Varghese, M. Paulose, K. Shankar, and C. a. Grimes, Sol. Energy Mater. Sol. Cells, 90, 14 (2006) 2011-2075.
20. Y. Li et al., Appl. Surf. Sci., 297 (2014) 103-108.
21. T. Ohsaka, F. Izumi, and Y. Fujiki, J. Raman Spectrosc., 7, 6 (1978) 321-324.
22. W. F. Zhang, Y. L. He, M. S. Zhang, Z. Yin, and Q. Chen, J. Phys. D. Appl. Phys., 33, 8 (2000) 912-916.
23. H. C. Choi, Y. M. Jung, and S. Bin Kim, Vib. Spectrosc., 37, 1 (2005) 33-38.
24. Y. Hara and M. Nicol, Phys. Status Solidi, 94, 1 (1979) 317-322.
25. B. Santara, P. K. Giri, K. Imakita, and M. Fujii, J. Phys. D. Appl. Phys.,47, 21 (2014) 215302,
26. Z. Lou, Y. Li, H. Song, Z. Ye, and L. Zhu, RSC Adv., 6, 51 (2016) 45343-45348.
27. X. Zhu, J. Chen, X. Yu, X. Zhu, X. Gao, and K. Cen, RSC Adv., 5, 39 (2015) 30416-30424.
28. Y. Fu, H. Du, S. Zhang, and W. Huang, Mater. Sci. Eng. A, 403, 1–2 (2005) 25-31.
29. Z. Fan, H. Guo, K. Fang, and Y. Sun, RSC Adv., 5, 31 (2015) 24795-24802.
30. Y. K. Kho, A. Iwase, W. Y. Teoh, L. Mädler, A. Kudo, and R. Amal, J. Phys. Chem. C, 114, 6 (2010) 2821-2829.

Садржај: *Једнодимензионе наноцеви TiO_2 усправно орјентисане на супстрат добијене су електрохемијском анодизацијом титанијумске фолије у киселом електролиту. У циљу промене кристалне структуре и морфологије филма, анодизовани аморфни*

филмови TiO_2 синтеровани су на високој температури. Морфолошка промена посматрана је скенирајућом електронском микроскопијом (СЕМ) док је кристална структура испитивана рендгенском анализом (ХРД) и Раманском спектроскопијом. Хемијски састав је урађен помоћу спектроскопске фотоемисије Х-зрака (ХПС). У овом раду је испитиван утицај кристалне структуре и морфологије нанотубуларног филма TiO_2 на фотокаталитичку деградацију воденог раствора метил оранжа (МО) под дејством ултраљубичастог зрачења. Наноцеви TiO_2 синтероване на 650 °C, 30 мин, показују најбољу кристалоичност и фотокаталитичку активност у поређењу са осталим филмовима TiO_2.

Кључне речи: *Титанијум диоксид; анодизација; синтеровање; кристална фаза; фотокатализа.*